Journal of Molecular Liquids 303 (2020) 112601

Contents lists available at ScienceDirect

Journal of Molecular Liquids

journal homepage: www.elsevier.com/locate/molliq

Aggregate formation in fluids with bounded repulsive core and competing interactions☆

Gianpietro Malescio [a,*], Francesco Sciortino [b]

[a] Dipartimento di Scienze Matematiche e Informatiche, Scienze Fisiche e Scienze della Terra (MIFT), Università di Messina, Viale F. Stagno d'Alcontres, 31, I-98166 Messina, Italy
[b] Dipartimento di Fisica, Università di Roma "La Sapienza", Piazzale A. Moro 5, I-00185 Roma, Italy

ARTICLE INFO

Article history:
Received 21 October 2019
Received in revised form 14 January 2020
Accepted 27 January 2020
Available online 31 January 2020

Keywords:
Self-assembly in complex liquids
Cluster formation
Non-homogeneous liquid phases
Soft matter
Fluids with microscopic competing interactions
Fluids with bounded repulsive core

ABSTRACT

Soft matter systems often exhibit an intriguing morphology, related to the formation of intermediate range order structures. A rationale proposed for this behavior is the presence of competing short-range attraction and long-range repulsion. On the basis that effective interactions among the centers of mass of soft macromolecules often result in a finite short-range repulsion, we here consider a model fluid in which competing interactions supplement a repulsive core that, at difference from the models investigated up to now, has a bounded nature. We study the structural and phase behavior of this model through a theoretical approach and by computer simulation. We find that the structure factor exhibits a low-k peak, which is particularly relevant at low densities, where our system is formed by polydisperse clusters. A distinctive feature characterizing our model fluid is the presence of a peak situated between the low-k peak and the first diffraction peak. We show that this second pre-peak is associated with the enhancement of the relative population of the second coordination shell with respect to the first one, generated at intermediate densities by the long-range repulsion. As it concerns the phase behavior, the system investigated undergoes, for weak long-range repulsion, a liquid-gas phase transition. Upon increasing the strength of the long-range repulsion, such transition becomes less evident and eventually disappears. At high densities, the system undergoes freezing into a clustered solid, with multiply occupied crystal sites.

1. Introduction

Soft matter systems often possess one or more frustrating interaction length scales driving micro- to mesoscale structural heterogeneity [1]. Examples include microemulsions [2], block copolymers [3–6], confined fluids [7,8], colloidal dispersions, proteins [9–13]. Despite their differences, all such systems exhibit similar transitions between homogeneous fluid states and emergent heterogeneous phases. One common feature of this class of morphologies is that the structure factor S (k) displays a characteristic pre-peak at a low but nonzero wavenumber [14–19]. Such modulated density fluctuations are related to the emergence of what is called intermediate-range order (IRO). Since this phenomenon can greatly impact the mechanical, optical, electronic, etc., properties of such systems, the ability to detect and characterize IRO structures is of great interest.

When dealing with complex materials as those above mentioned, it is useful to resort to model systems in order to simplify their study. Commonly used model systems are particles with isotropic interactions. Even though this is often an oversimplification of most real systems, information obtained from these model systems has been shown to be crucial to understand many soft matter materials. Recently, there has been an increasing interest in studying isotropic model systems characterized by an infinitely repulsive core plus a short-range attraction and a long-range repulsion (SALR systems) [10,17,19–26]. Frustration deriving from the competing short-range attractive and long-range repulsive components of the interparticle interactions has been shown to give rise to spontaneous micro-separated fluid phases [16,19,22], as well as microphases with long-range, periodic order [27,28], with the introduction of new phases into the phase diagram, such as clustered fluid, cluster percolated fluid, cluster glass etc.. Understanding how, by controlling the parameters of the SALR interaction, it is possible to influence self-assembling processes, and thus the clusters nature, is fundamental in order to characterize and eventually engineer IRO structures, which can lead to new way to synthesize materials [29–32].

When considering interactions among macromolecules, the effective interparticle interactions may often result in a bounded short-range repulsion that allows the particles to "sit on top of each other", imposing only a finite energy cost for a full overlap. Such potentials arise naturally as effective interactions between the centers of mass of soft, flexible macromolecules such as polymer chains [33], dendrimers [34], polyelectrolytes, etc. Indeed, the centers of mass of two macromolecules can coincide without violation of the excluded volume

☆ This article was accepted for publication under the special issue collection CPBCI 2019.
* Corresponding author.
E-mail address: malescio@unime.it (G. Malescio).

https://doi.org/10.1016/j.molliq.2020.112601
0167-7322/

conditions, hence bringing about a bounded interaction. For example, a well-known model able to describe in an excellent approximation interactions between the centers of mass of two polymer chains in an athermal solvent is the so-called GCM (Gaussian core model), where the intermolecular potential has a repulsive Gaussian form [35].

In this paper we consider a model fluid with a Gaussian repulsive core followed by an attractive well and a long-rage repulsive component, both having a Gaussian form. Though this model currently does not represent any existing realistic colloidal system, novel macromolecules and colloidal particles can nowadays be synthesized with quite complex interaction potentials. Thus, when studying aggregation and microphase formation in soft matter, it appears of considerable interest to investigate systems having a penetrable internal "core" represented through a bounded repulsion, supplemented by competing interactions.

We investigate the structural properties and the phase behavior of the system considered by using a theoretical approach based on the hypernetted-chain integral equation, and through Molecular Dynamics and Grand Canonical Monte Carlo simulations. We find that the structure factor of the system considered exhibits a low-k peak, which is particularly relevant at very low densities. In this regime, through a cluster analysis, we show that the system is formed by polydisperse clusters. At intermediate densities, the structure factor of our model fluid exhibits a novel feature, never observed in SALR systems, i.e. a second pre-peak, located between the low-k peak and the first diffraction peak and thus related to correlations over a length scale intermediate between cluster-cluster correlations and monomer-monomer correlations. We present an analysis that allows to associate this peak with the role played by LR repulsion in giving origin at small densities to partially excluded volume effects.

We studied the phase behavior of the model investigated, and showed that when the long-range repulsion is weak with respect to the short-range attraction, the system undergoes, at low densities, a liquid-gas transition. As the long-range repulsion increases, the instability region related to the liquid-gas transition shrinks moving towards lower temperatures and densities. Accordingly, the peak of S(k) at $k = 0$, which is typical of a system close to a liquid-gas transition, gradually decreases, and a local peak develops at $k \neq 0$, i.e. the system goes from a simple fluid-like behavior to an "intermediate range order" behavior.

At high densities the system considered undergoes freezing into a clustered solid, characterized by multiply occupied crystal sites. The solid region of the thermodynamic plane rapidly increases as the long-range repulsion gets stronger.

2. The model

We consider a system of particles interacting through the following potential:

$$U(r)/\epsilon = \exp\left(-\left(\frac{r}{\sigma}\right)^2\right) - w\cdot \exp\left[-\left(\left(\frac{r}{\sigma}\right)-2\right)^2\right] + \alpha\cdot \exp\left[-((r/\sigma)-3)^2\right]\cdot f(r) \quad (1)$$

where r is the interparticle distance, ε and σ are arbitrary energy and length units, respectively, w and α are the strength of the short-range attraction and of the long-range repulsion, respectively, and $f(r)$ is the function:

$$f(r) = \frac{1}{1 + \exp\left[\frac{3-(r/\sigma)}{0.1}\right]} \quad (2)$$

Temperature and density are expressed in units of ϵ and σ^{-3}. Throughout our investigation $\epsilon = 1, \sigma = 1, w = 0.05$.

The potential $U(r)$ defined in Eq. (1) is composed of three terms: a finite repulsive core having the form of a Gaussian centered at the origin, an attractive component consisting in a negative Gaussian centered at $r = 2$ having fixed strength w, and a repulsive long-range term which is given by the product of a Gaussian centered at $r = 3$ times the function $f(r)$, which is a continuous function approximating a Heaviside step function that goes from 0 to 1 around $r = 3$. This specific form of the long-range repulsion makes it possible to vary its strength, i.e. α, without significantly affecting the inner repulsion and attraction. The potential $U(r)$ is shown in Fig. 1 for a few values of α.

3. Methods

To investigate the behavior of the system considered we make use both of theoretical and computational approaches.

3.1. Theory

As a manageable theoretical tool apt for an extensive investigation, we turn to the hypernetted-chain (HNC) integral equation. Integral equations are based on the Ornstein-Zernike (OZ) relation [36], that for a homogeneous and isotropic fluid is:

$$h(r) = c(r) + \int d^3r'\, c(r')\rho h\left(|\vec{r} - \vec{r'}|\right) \quad (3)$$

which, by taking the Fourier transform, becomes

$$h(k) = c(k) + \rho c(k)h(k) \quad (4)$$

The OZ relation is an exact relation describing the fact that the total correlation between particles 1 and 2, represented by $h(r) = g(r) - 1$, where $g(r)$ is the pair distribution function, is due in part to the direct correlation between 1 and 2, represented by $c(r)$, but also to the indirect correlation, represented by the integral in the above expression, propagated via increasingly large numbers of intermediate particles. To solve the OZ relation one needs an additional relation linking $h(r)$ and $c(r)$ (called closure relation). Since the exact closure is unknown, several approximate relations have been proposed, each leading to a specific integral equation. The closure leading to the so-called hypernetted-chain (HNC) integral equation is obtained by neglecting a certain class of

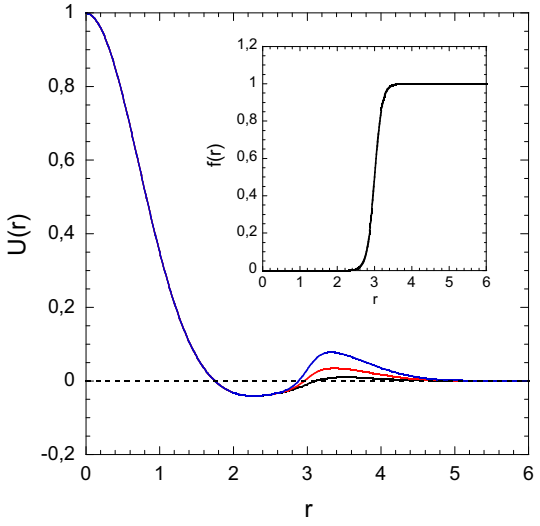

Fig. 1. Interaction potential U(r) defined in Eq. (1); $\alpha = 0.02$ (black solid line), 0.05 (red line), 0.1 (blue line). For $\alpha = 0.05$, $U(r_{min}) = -0.04$ while $U(r_{max}) = 0.035$, where $r_{min} = 2.27$ and $r_{max} = 3.36$. The function f(r) is shown in the inset.

diagrams (bridge diagrams) in the expansion of $g(r)$ and reads [36]:

$$g(r) = h(r) + 1 = e^{-\beta U(r)+h(r)-c(r)} \quad (5)$$

which is equivalent to

$$c(r) = h(r) - \ln[h(r) + 1] - \beta U(r) \quad (6)$$

The solution of the OZ relation with the HNC closure is obtained through a numerical iterative procedure. From an initial guess for, say, c(r), one calculates the Fourier transform c(k), which is used in Eq. (4) to obtain h(k). Its inverse Fourier transform provides a new estimate of h(r) and, through Eq. (6), of c(r), which is used as a new input for the next cycle. The functions are evaluated on a spatial grid with $\Delta r = 0.01\sigma$ (where σ is the length scale) and N = 2048 points. Checks with $\Delta r = 0.005\sigma$ and N = 4096 were also performed.

In general, the HNC equation has well-known limits related mainly to its thermodynamic inconsistency. However, it proved to be very effective in describing the thermodynamics and structure of particles interacting through a bounded repulsive pair potential [35]. Thus, it represents a valuable tool for a large-scale investigation of potentials with competing interactions and a penetrable core as that considered here.

The HNC equation can be solved in a region of thermodynamic parameters ("stable" region). This is separated from the region where no solution is found ("unstable" region) by a boundary line (BL). For ordinary simple fluids, characterized by a diverging short-range repulsion, the BL can be associated with the liquid-vapor spinodal line, marking the threshold of instability towards phase separation. While the spinodal line is characterized by the divergence of the isothermal compressibility χ_T, upon approaching the BL the isothermal compressibility increases without exhibiting a true divergence, whence the name "pseudospinodal line" also reserved to the BL. Recently, the BL of the HNC equation was computed for a number of model interactions with bounded repulsive core supplemented by a short-range attraction [37–39]. When compared to the binodal line calculated through MC simulation, the BL yielded fairly reasonable results. In particular, the binodal line and the BL show analogous topological modifications upon changing the attraction strength.

Moreover, the HNC equation proved able to predict a peculiar kind of freezing occurring in systems characterized by bounded repulsive interactions that decay fast enough to zero as the interparticle distance goes to infinite (as the penetrable sphere model (PSM) [40,41]). In this case, the solid can always lower its free energy, as density increases, by allowing more and more particles to occupy the same lattice sites. This clustering mechanism stabilizes then the solid at all temperatures and a practically constant effective density of clusters is maintained in the crystal. It was shown for the PSM, that the BL of the HNC equation compares well with the fluid–solid coexistence curve obtained through a density-functional approach [42].

3.2. Simulation

We have investigated the properties of the model via Molecular Dynamics (MD) and Grand Canonical Monte Carlo (GCMC) simulations. MD simulations have been performed with a standard home-written code in the NVT ensemble, with the specific aim to quantify structural information for a system of at least N = 1000 particles in three dimensions. The integration time-step is 0.01. GCMC simulations have also been performed with a home-written code with the aim of evaluating the gas-liquid coexistence. Random displacement moves with amplitude between $\pm 0.025\ \sigma$ were randomly alternated with particle insertion and deletion moves.

To efficiently evaluate the probability P(N,T,μ) and locate the gas-liquid coexistence we implemented the successive umbrella sampling (SUS) method [43]. P(N,T,μ) indicates the probability that in the simulated volume there are N particles when the system is constrained to a temperature T and chemical potential μ. As such, the logarithm of P(N, T,μ) is proportional to the Helmholtz free energy of the system. Coexistence between two phases requires a two peak distribution for P(N,T,μ), with equal area below each peak. To cover the density interval $0 < \rho < 0.13$ we performed 600 independent grand-canonical simulations of a box of side L = 17 constrained to explore only systems with N or N + 1 particles, with N varying from 0 to 599. Each simulation, lasting at least 1 million attempts to insert or delete a particle and at least 100 million attempts to randomly displace a particle, provides the ratio P(N + 1,T,μ)/P(N,T,μ). Combining all 600 simulations, the entire P(N,T,μ) is rebuilt. Preliminary runs at different temperatures are used to identify the region where the density fluctuations are bimodal, an indication of two-phase coexistence. Eventually, runs have been performed for T = 0.03, 0.04, 0.045, 0.048, 0.0483, 0.0485, 0.05.

More detailed information on the SUS method and application to colloidal particles can be found in [44,45].

4. Results and discussion

4.1. Structural properties

We first calculated, by using the HNC equation, the structure factor S(k) and the radial distribution function g(r) of a system of particles interacting through the potential described by Eq. (1), for a fixed strength of the long-range repulsion, $\alpha = 0.05$, at a fixed temperature T = 0.03, and for several densities (Fig. 2).

In order to assess the reliability of the HNC equation as it concerns the system considered, we compared the structure factors calculated through the HNC equation with those obtained through MD simulation (see Fig. 3). The predictions of the HNC equation are found to be in good agreement with the results of MD simulation.

We then considered the same system at a lower temperature (T = 0.01). At this temperature, the HNC equation cannot be solved at very small densities and for $\rho \geq 0.4$ (the extent and the topology of the unstable region of the HNC equation will be discussed in Section 4.3). So we calculated the structure factor S(k) and the radial distribution function g(r) at T = 0.01 by using the MD simulation.

Upon examining the structure factors of the system investigated both at T = 0.03 and T = 0.01, it is possible to note, with varying density, the gradual turning on and off of different length scales (see Fig. 2 left panel, Fig. 4 upper panel). At low densities ($\rho \sim 0.01$) the highest peak is centered around $k \cong 1$. Then, as density increases, this peak goes down and at intermediate densities ($\rho \sim 0.1$–0.2 depending on T) the highest peak is that centered at $k \cong 3$. As density further increases, also this peak decreases, and at high densities ($\rho > 0.25$) the highest peak is that centered around $k \cong 5$. The value of the peak at $k \cong 5$ is always greater than one, and grows monotonically with the density. To make evident the above described behavior, we plotted, for T = 0.03, the height of the peaks centered respectively at $k \cong 1$, $k \cong 3$, $k \cong 5$, as function of the density (Fig. 5).

As follows from Fig. 5, the peak at $k \cong 1$ (first pre-peak) is associated to correlations that are relevant in a restricted range of densities and lose importance for $\rho > 0.1$. The peak at $k \cong 3$ (second pre-peak) is associated to correlations that are relevant over a broader range of densities, but tend to vanish too at high densities (say, $\rho > 0.5$). On the contrary, the peak at $k \cong 5$ is related to correlations that become more important with the density. For $\rho > 0.5$, as the region where crystallization occurs (see Fig. 11 and the discussion in Section 4.3) is approached more and more closely, this peak exhibits a more and more rapid increase. The length scale associated to the position of the third peak ($L = 2\pi / k \sim 1.2$) corresponds approximately to the effective diameter of the inner repulsive core of our model. In a dense packing regime, the excluded volume effects associated to the particle core are dominant, and the additional components of the interaction potential, i.e. the short-range attraction and the long-range repulsion, play a minor role. In the light of the preceding considerations, the peak at $k \cong 5$ is to be

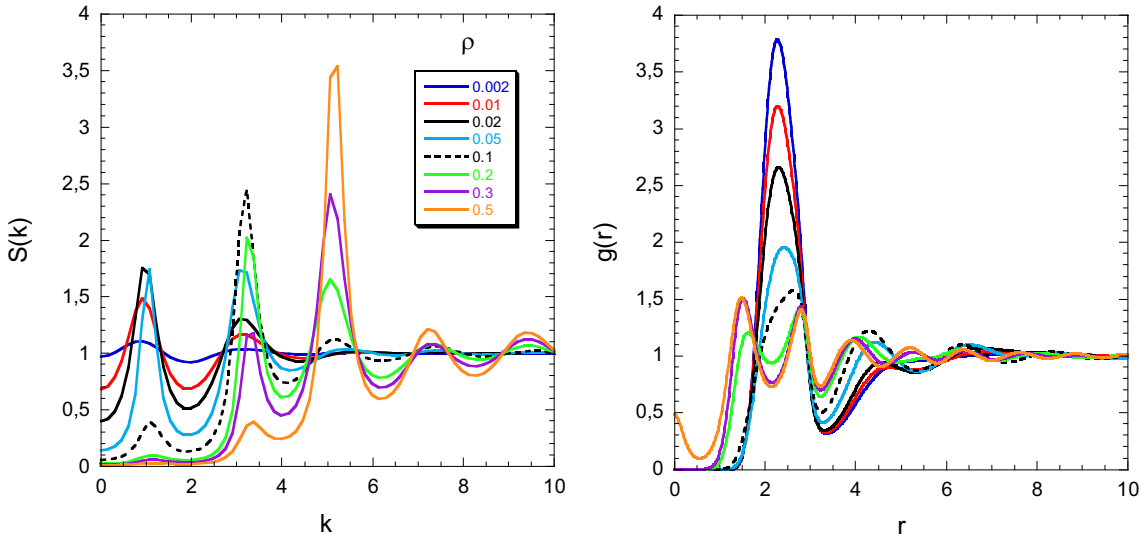

Fig. 2. Structure factor S(k) (left panel) and radial distribution function g(r) (right panel) calculated through the HNC equation for several densities at T = 0.03; α = 0.05.

regarded as the main diffraction peak associated to "monomer-monomer" correlations.

The appearance in the interparticle structure factor of a peak whose position is at smaller wave-vectors than the position of the main diffraction peak, has been related in the literature to the emergence of intermediate range order (IRO). The low-k peak, termed IRO peak, is a characteristic feature of many SALR systems [10,15,18,26]. It has been initially attributed to the correlation between clusters with preferred size in solutions [10]. However, it was later argued that the relationship between the low-k peak and the particle arrangement is not so straightforward [11,46–48]. In general, the existence of an IRO pre-peak appears to be a necessary but not sufficient evidence for identifying a clustered phase [48]. Provided a cluster phase occurred, the real-space length scale $2\pi/(k_{IRO})$, corresponding to the position k_{IRO} of the low-k pre-peak, can be interpreted as the average center-to-center real-space intercluster distance [49].

In the system here investigated, the structure factor shows, in addition to the first or low-k pre-peak, a second evident pre-peak situated between the low-k peak and the main diffraction peak. This is a novel feature never observed in SALR model systems before [50]. Depending on density and temperature, both the first and the second pre-peak may attain maximum values much greater than one. As shown in Fig. 5, the second pre-peak is particularly relevant at intermediate densities, where the usual low-k pre-peak is considerably smaller than one and the main peak is still only slightly greater than one. This behavior gets more and more evident as temperature is lowered (see Fig. 6). Though, as shown in Fig. 5, the two pre-peaks and the main peak attain their maximum relevance in different density regimes, for some values of the thermodynamic parameters (e.g. T = 0.01, $\rho \sim 0.05$) the three peaks are simultaneously well evident with a maximum value greater than one for all of them (Fig. 4 upper panel).

As mentioned above, many efforts have been devoted to understanding the relationship between the occurrence of the IRO peak and the cluster formation. Being able to describe cluster morphologies by decoding S(k) is highly desirable because it would make possible to obtain knowledge about multi-body structure based on pair correlations; it is also of practical interest because measurements of pair correlations are feasible for many soft matter systems and length scales. In order to analyze the possible aggregation of particles with the formation of clusters, we calculated, through MD simulation, the probability distribution P(s) of observing a cluster of size s at T = 0.01 for several densities (Fig. 7) before the percolation threshold. Particles have been considered as bonded if their distance is smaller than the position of the maximum r_{max} of the long-range repulsive component of the interaction (r_{max} = 3.36). Particles are considered to be part of the same cluster if there is a continuous path of bonds connecting them.

We first consider a very low value of density ($\rho = 0.002$) and find that P(s) has two local maxima, one at s = 1 (single particles) and the other at s = 6. The second maximum indicates the presence of clusters formed preferentially by six particles. Since the two maxima have approximately the same height, clusters coexist with a low-density population of monomers. As the density increases, the tendency to aggregation becomes more evident (Fig. 8, upper panel). At $\rho = 0.01$, the presence of single particles, as well as that of small clusters (formed by 2–3 particles) becomes less probable. As a consequence, the peak of P(s) around s = 6–7 becomes more evident. At the same time, given the higher density, the presence of clusters formed by more than 7 particles becomes more probable. It follows that the system is mostly formed by polydisperse clusters with a preferred cluster size s = 6–7 (Fig. 8, bottom panel).

On further increasing density, the polydispersity increases and the cluster size distribution approaches for largest power-law behavior expected in the proximity of a percolation transition. For all the shown densities, the system can be described as formed by polydisperse clusters interacting through a repulsive potential. We find that at $\rho = 0.03$ the system percolates and all particles belong to the same spanning cluster. At T = 0.01 and $\rho = 0.002$ the first pre-peak (centered at $k \cong 1$) attains a maximum value of about 2.5. This value rises to about 4 for T = 0.01 and $\rho = 0.01$. The results shown in Fig. 7 thus are in agreement with an empirical criterion proposed in [19], stating that when in SALR system the height of the low-k pre-peak reaches a value ≥ 2.7, the pre-peak is to be associated with the emergence of clustering.

To get additional insight about the nature of clustered structures, we investigated how the average potential energy varies with the density of the system (Fig. 9). We observe a shallow minimum at low densities (around $\rho \sim 0.03$), where the potential energy is negative. Indeed, at low densities the g(r) has a remarkable peak at r ≈ 2.2–2.3, in correspondence with the minimum of the attractive well. This gives origin to a negative average potential energy. As the density increases, this peak decreases and shifts towards the right extreme of the well where attraction is weaker. However, being the excess energy per particle given by

$$U_{ex}/N = 2\pi\rho \int_0^\infty v(r)g(r)r^2 dr, \tag{7}$$

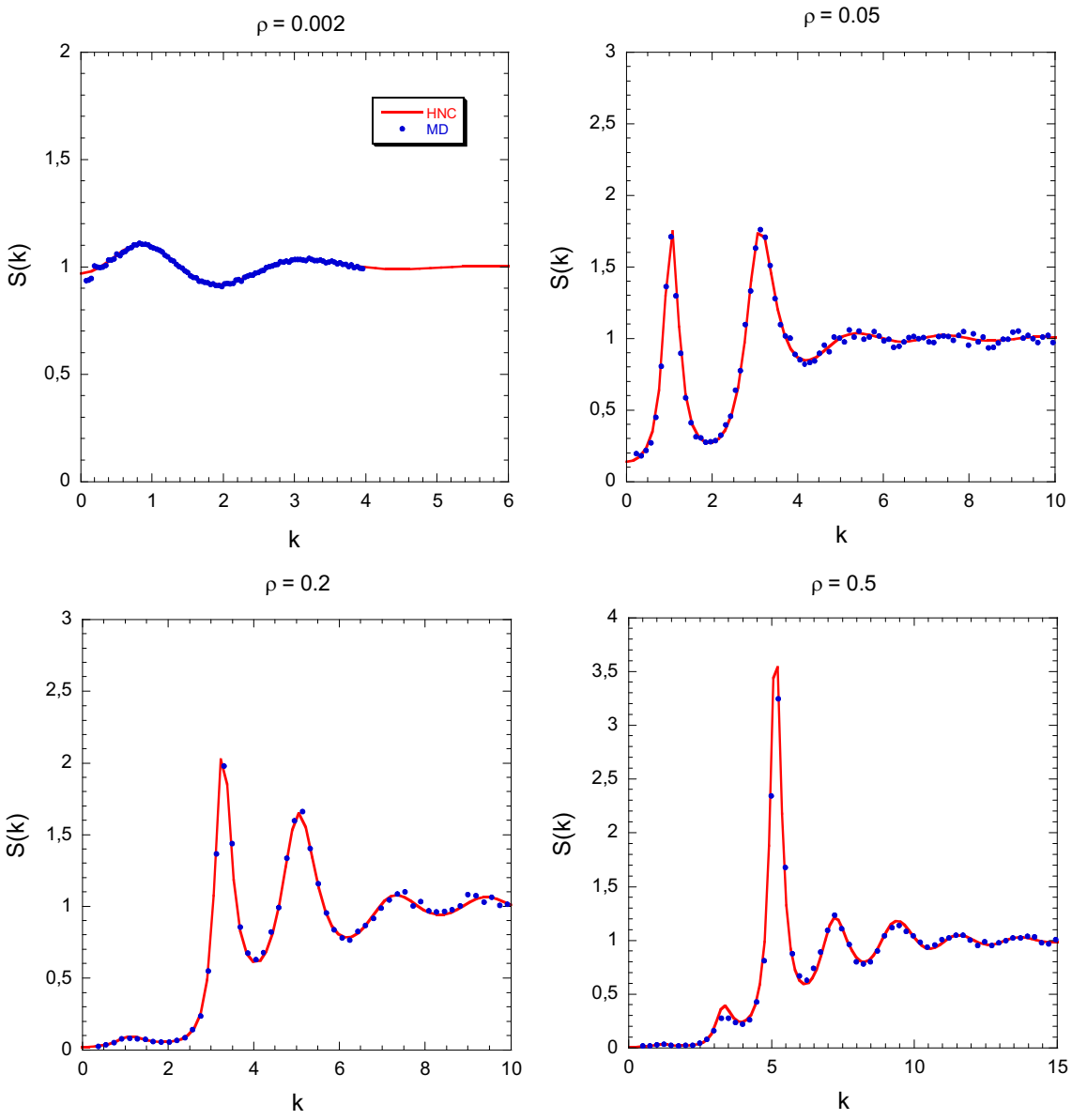

Fig. 3. Comparison between the S(k) calculated through the HNC equation and that obtained through MD simulation for several densities at T = 0.03; α = 0.05.

This effect is compensated by the factor r^2, so the potential energy remains essentially constant. For densities above $\rho \approx 0.05$, the attractive well gets less and less populated while a new peak develops in the g(r) for $r < 2$, where the potential is repulsive. Consequently, the potential energy increases and turns positive at $\rho \approx 0.08$. As density further increases, overlapping of the tail of the internal repulsive core of the particles becomes more and more relevant and the potential energy keeps growing with the density.

Let us now turn our attention to the second pre-peak of the structure factor. This is to be related to correlations over a length scale intermediate between those associated to the first pre-peak and to the monomer-monomer peak, respectively. Though a second pre-peak has never been observed in model systems with SALR interactions, scattering experiments showed the existence of a second pre-peak, in addition to the low-k pre-peak, in ionic liquids [51–54]. This second pre-peak has been associated with distances between ions of similar charge, so it has been called charge alternation peak [54].

In order to interpret the meaning of the second pre-peak in our system, we carefully analyze the behavior of the radial distribution function. We focus on the g(r) reported in the right panel of Fig. 2 (α = 0.05, T = 0.03). At very low densities, g(r) has a high peak in correspondence with the position of the attractive well (r ≈ 2.2). As density increases, this peak decreases, while a second peak develops just on the tail of the LR repulsion (r ≈ 4.5). The position r_1 of the minimum of g(r) that separates these two peaks corresponds approximately to the maximum of the LR repulsion. The second peak of g(r) attains its maximum value at ρ ≈ 0.1, after which it decreases and shifts towards slightly smaller values of r (r ≈ 4). For ρ ≥ 0.2, the first peak of g(r) splits into two peaks, whose positions correspond approximately with the left and right extremes of the well, while for ρ > 0.4 a whole new peak develops at r = 0.

To highlight the consequences of the above outlined changes of the g(r), we calculate the quantities n_1 and n_2 given by:

$$n_1 = 4\pi\rho \int_0^{r_1} g(r) r^2 dr \qquad n_2 = 4\pi\rho \int_{r_1}^{r_2} g(r) r^2 dr \tag{8}$$

where r_1 has been defined above, and r_2 is the position of the minimum that follows the peak laying on the tail of the LR repulsion. For ρ < 0.2, n_1 and n_2 are the coordination number of the first and of the second shell,

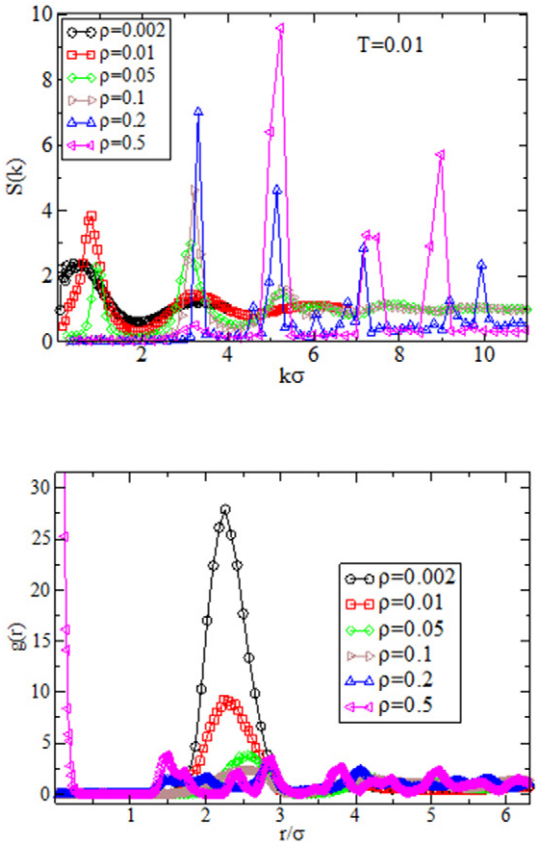

Fig. 4. Structure factor S(k) (upper panel) and radial distribution function g(r) (bottom panel) calculated through MD simulation for several densities at T = 0.01; α = 0.05. As signaled by the position and height of the peaks in the structure factor and in the radial distribution function, at densities ρ = 0.2 and beyond, the system crystallizes.

respectively. This is no more true at higher densities, where new shells appear for $r < r_1$. Thus, for $\rho \geq 0.2$, n_1 represents the number of particles inside a sphere of radius r_1 centered in the origin (region 1), and n_2 is the number of particles inside the shell between r_1 and r_2 (region 2).

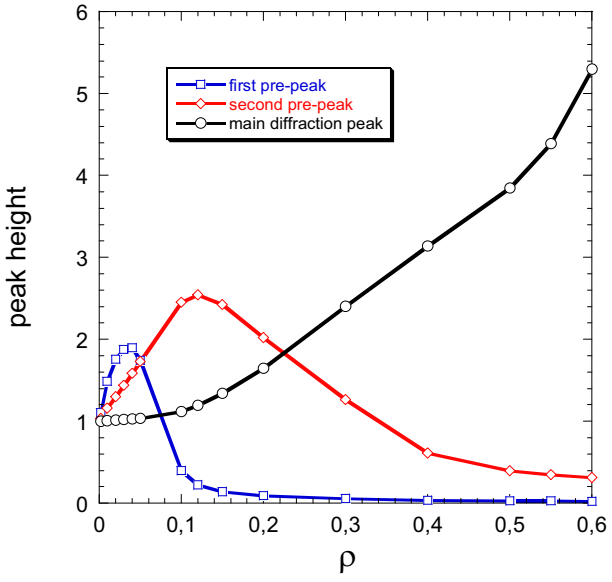

Fig. 5. Maximum height of the first and second pre-peak, and of the main diffraction peak of S(k) as function of the density at T = 0.03; α = 0.05. S(k) was calculated through the HNC equation.

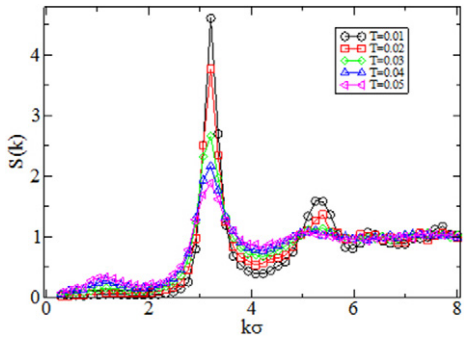

Fig. 6. Structure factor S(k) calculated through MD simulation at $\rho = 0.1$, for several temperatures; $\alpha = 0.05$.

As shown in Fig. 10, n_1 grows with the density following an approximately linear behavior over the whole density range considered. The behavior of n_2 is more variegated: two distinct regimes can be identified, one at low densities ($\rho \leq 0.1$) with a rather fast growth, and one at larger densities ($\rho \geq 0.3$) with a less rapid growth and an approximately linear behavior. The transition between the two regimes occurs in the interval $0.1 \leq \rho \leq 0.3$. In the inset of Fig. 10 we report r_1 and r_2 as function of density. While r_1 is approximately constant, r_2 depends more significantly on the density and has a maximum at $\rho \approx 0.1$.

In order to compare the relative occupation of the two regions, we consider the ratio $R = n_2/n_1$ (Fig. 10). This quantity at first rapidly increases with the density, reaches a maximum at $\rho \approx 0.1$, and then decreases approaching an approximately constant value. This behavior makes clear that at $\rho \approx 0.1$, the second shell has, relatively to the first one, a maximal occupation. Since the two regions are separated by the minimum of g(r) roughly corresponding to the maximum of the LR repulsion, a rationale for the observed behavior is the following. The LR repulsion acts as a barrier partially hindering the penetration of particles into the inner regions of the potential. It follows that the accumulation of particles in region 2 (corresponding, for $\rho < 0.2$, to the second shell) is more and more favored, relatively to region 1 (corresponding, for $\rho < 0.2$, to the first shell), up to a given density ($\rho \approx 0.1$), where R reaches its maximum value, while for larger densities, the LR repulsion, due to its finite nature, becomes less and less effective. The relevant feature of the behavior of R is not the magnitude of its maximum value, which depends mainly on the extension of region 1 and region 2, but the rapidity of its increase with density at small densities (and the subsequent decrease for $\rho > 0.1$). The peculiarity of the behavior of R can be highlighted through the comparison with the ratio R between the coordination number of the second shell to that of the first one for well-known potentials such as the Lennard-Jones potential or the hard sphere + square well potential. At difference from the potential considered here, in both cases R does not vary significantly with the density.

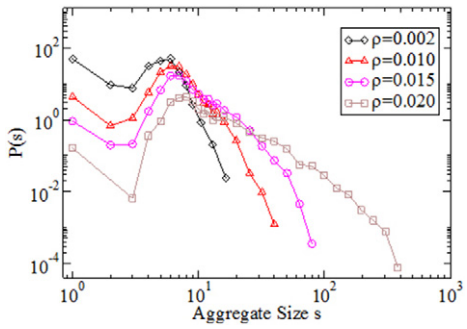

Fig. 7. Cluster size distribution P(s) at T = 0.01, for several densities; α = 0.05. P(s) is normalized such that Σ sP(s) = N, where N = 1000 is the total number of particles in the simulation. Calculations were performed through MD simulation.

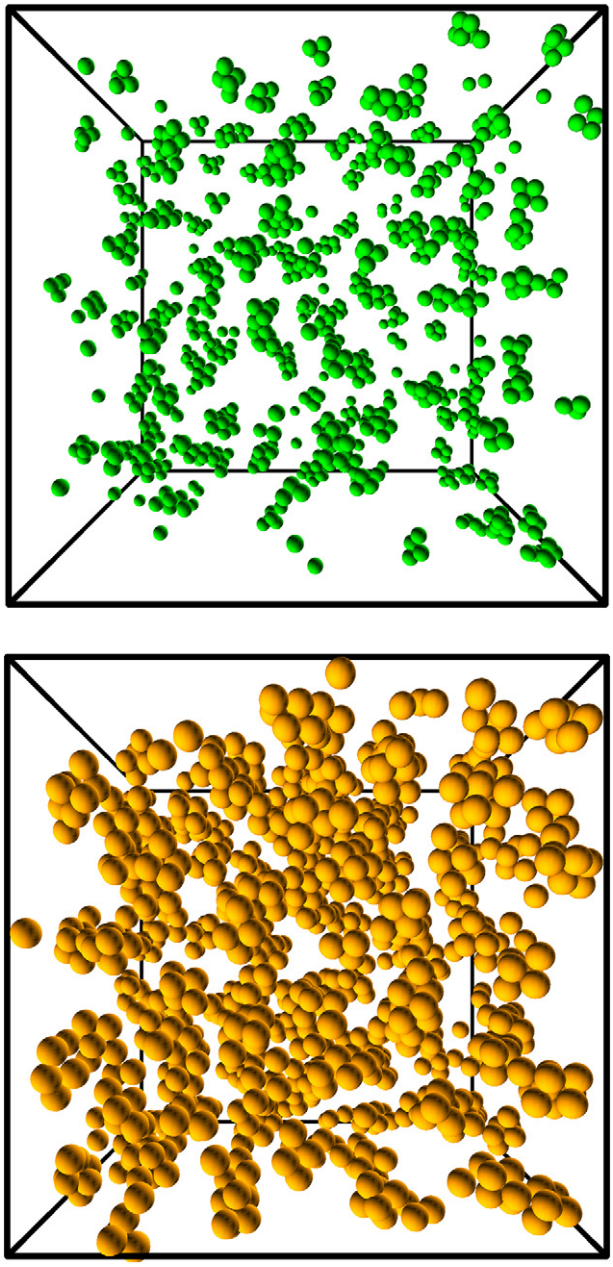

Fig. 8. Snapshots of the system in the cluster phase at T = 0.01 and ρ = 0.002 (upper panel) and ρ = 0.010 (bottom panel). In these snapshots the diameter of the particles is 2.4 σ, corresponding to the minimum of the pair interaction potential.

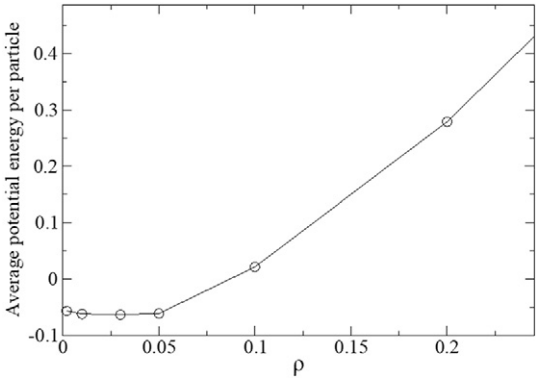

Fig. 9. Potential energy per particle as a function of density; T = 0.01, α = 0.05. Calculations were performed through MD simulation.

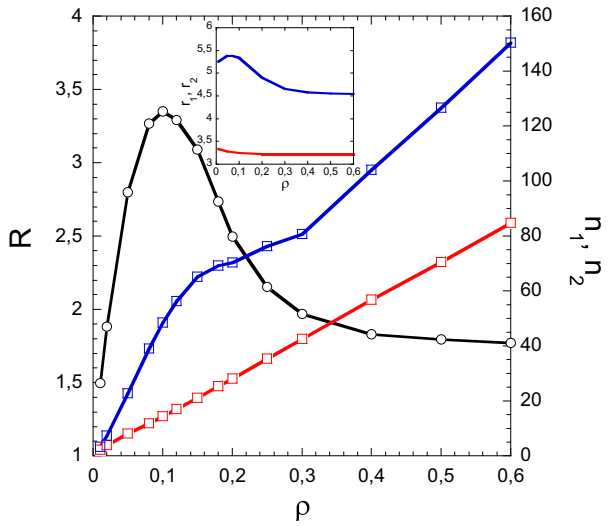

Fig. 10. Number n_1 of particles inside region 1 (red line), number n_2 of particles inside region 2 (blue line), and ratio R of n_2 to n_1 (black line), as function of the density; α = 0.05, T = 0.03. The radial distribution functions used to determine n_1 and n_2 were calculated using the HNC equation. Inset: r_1 (red line) and r_2 (blue line) as function of the density.

As shown by the above analysis, there exists a density range (centered around ρ ≈ 0.1 for α = 0.05, T = 0.03) where the occupancy of the second coordination shell with respect to the first one is significantly larger than for other densities. In such regime, the second pre-peak of S(k) is the dominant peak. Thus we posit that this peak is associated with the role played by LR repulsion as a barrier determining partially excluded volume effects. Given the finite nature of the LR repulsion, its efficacy to this regard becomes lower and lower at larger densities. In principle, such effect, and the related presence of the second pre-peak, might occur also in SALR potentials with diverging repulsive core. We performed a preliminary exploration of the parameter space of a potential consisting in a hard-sphere repulsion plus a square well attraction and a repulsive ramp, and found that a second pre-peak is generally absent. Only for few attentively selected sets of parameters we observed a second pre-peak, but it is always scarcely relevant, at difference from the system here investigated. A possible explanation is that, due to the infinitely repulsive nature of the inner core, the effect of the LR repulsion on the particle spatial arrangement, at least as it concerns the above described phenomenon, is totally or partially masked by the stronger core-core correlations.

4.2. Structural properties: varying the strength of the long-range repulsion

To investigate the role played by the competition between the short-range attraction and the long-range repulsion, we calculated, through the HNC equation, the structure factor S(k) for several values of the strength α of the long-range repulsion, at T = 0.05 and for several densities (Fig. 11). We chose a somewhat higher temperature with respect to previous calculations, in order to ensure that the HNC equation can be solved for all the values of α considered (except for α = 0.1 at ρ = 0.4). The extension and nature of the instability region of the HNC equation will be thoroughly studied in Section 4.3.

In general, the structure factor of a homogeneous fluid is finite for all wavevectors k. The appearance of a divergence in S(k) signals an instability with respect to density fluctuations. If the divergence occurs at k = 0, macroscopic phase separation ensues, which in liquid-state theory typically corresponds to the gas−liquid spinodal. A divergence at k > 0 signals instability with respect to mesoscale fluctuations, which

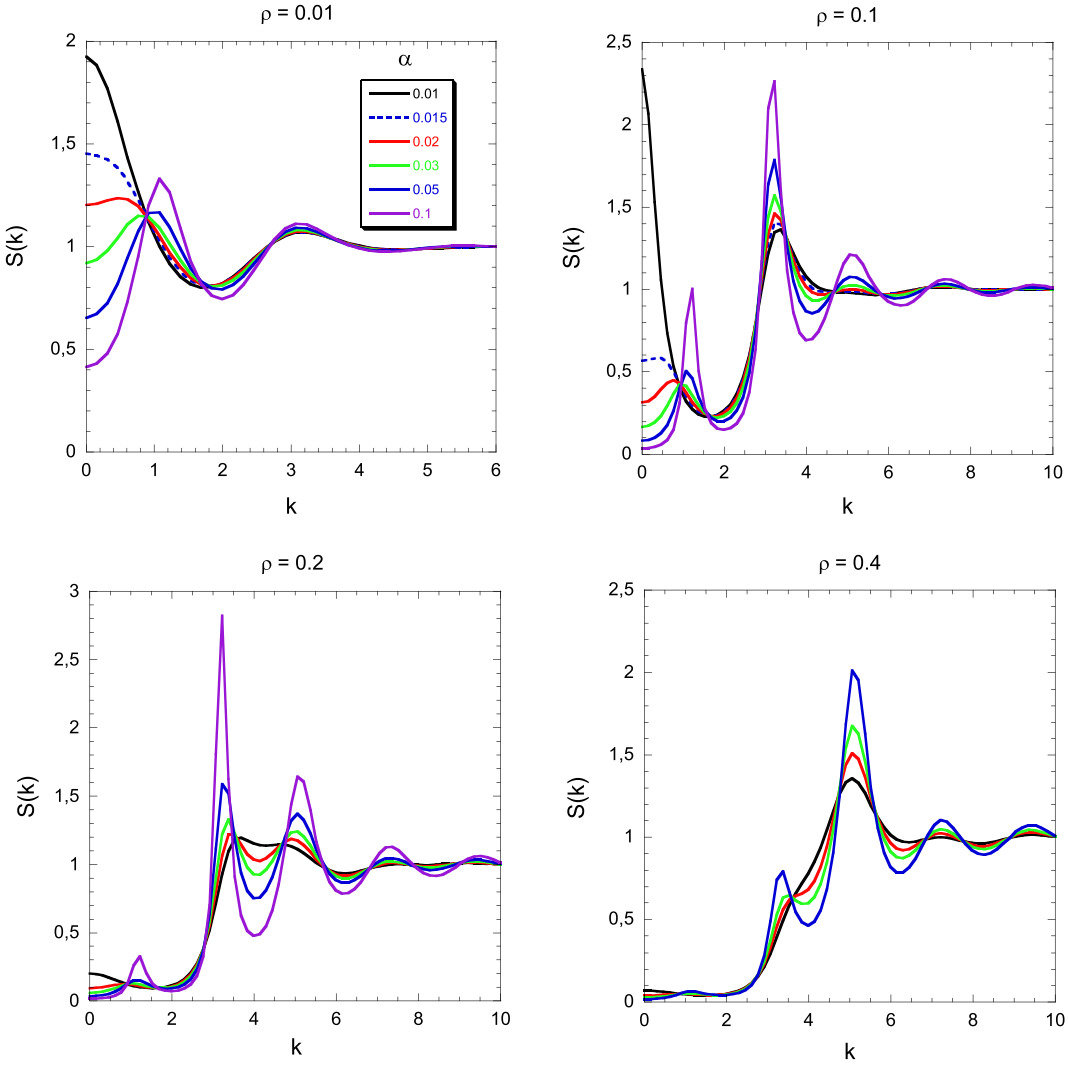

Fig. 11. Structure factor S(k) calculated through the HNC equation for several densities at T = 0.05, for several values of α.

indicates the presence of a periodic microphase regime. These two different behaviors are separated, in the space of the model parameters, by the Lifshitz point. Below this point, the loss of stability of density fluctuations occurs at k = 0 and the system behaves as a simple fluid. Above the Lifshitz point, the competition between short-range attraction, that favors the formation of aggregates at low temperatures, and long-range repulsion, that frustrates a complete phase separation, gives rise, below a certain temperature, to a micro-separated, locally non-homogeneous fluid with modulated phases characterized by large density fluctuations at k > 0.

When $\alpha = 0$, the interaction defined in Eq. (1) consists just in a Gaussian repulsive core plus the short-range attraction. The corresponding system undergoes a liquid-gas transition, which is associated to the increase of density fluctuations, and thus of the isothermal compressibility χ_T. This, in turns, gives origin to a peak in the structure factor at k = 0, as it follows from the well-known relation

$$S(k=0) = \rho k_B T \chi_T \tag{9}$$

This behavior persists as far as the long-range repulsion is weak with respect to the short-range attraction. As shown in Fig. 11, S(k) has, for $\alpha = 0.01$ or smaller, an evident peak at k = 0 for low densities ($\rho < 0.2$), which is typical of a system close to a liquid-gas transition. By increasing α, the peak of S(k) at k = 0 gradually decreases, the zero-wavenumber convexity switching from negative to positive, and eventually a local peak (first pre-peak) develops at $k \cong 1$. Thus, the system goes from a simple fluid – like behavior to an "intermediate range order" behavior typical of a microseparated, locally non-homogeneous fluid. At very low densities ($\rho = 0.01$), and for $\alpha \geq 0.03$, the peak at $k \cong 1$ is the highest one. At $\rho = 0.1$, the peak at $k \cong 1$ is considerably lower, and the second pre-peak (around $k \cong 3$), which is now the dominant one, becomes higher and higher by increasing α. A third peak (the main diffraction peak), centered around $k \cong 5$, becomes evident for sufficiently large values of α. At $\rho = 0.2$, for very small values of α, the structure factor shows, in addition to the peak at k = 0, a wide peak centered around $k \cong 4$. As α increases, this peak splits into two parts, giving origin to two well separated peaks, one at $k \cong 3$ and the other at $k \cong 5$. At $\rho = 0.4$, the highest peak is that at $k \cong 5$. Its height increases with α, as well as that of the peak centered at $k \cong 3$. At such density, the peak at $k \cong 1$ is scarcely evident. At even higher densities (not shown in the figure), the peak at $k \cong 5$ is the dominant one at all α's, the peak at $k \cong 3$ is barely evident, and that at $k \cong 1$ is totally absent. As it follows from Fig. 10, at all densities (except at the smallest one, $\rho = 0.01$, where the main effect of the LR repulsion is the suppression of the peak at k = 0 and the emergence of the peak at $k \cong 1$), by increasing α both the two pre-peaks and the main peak become more and more evident. At intermediate densities ($\rho \sim 0.1$–0.2 depending on T), this effect is particularly evident on the second pre-peak.

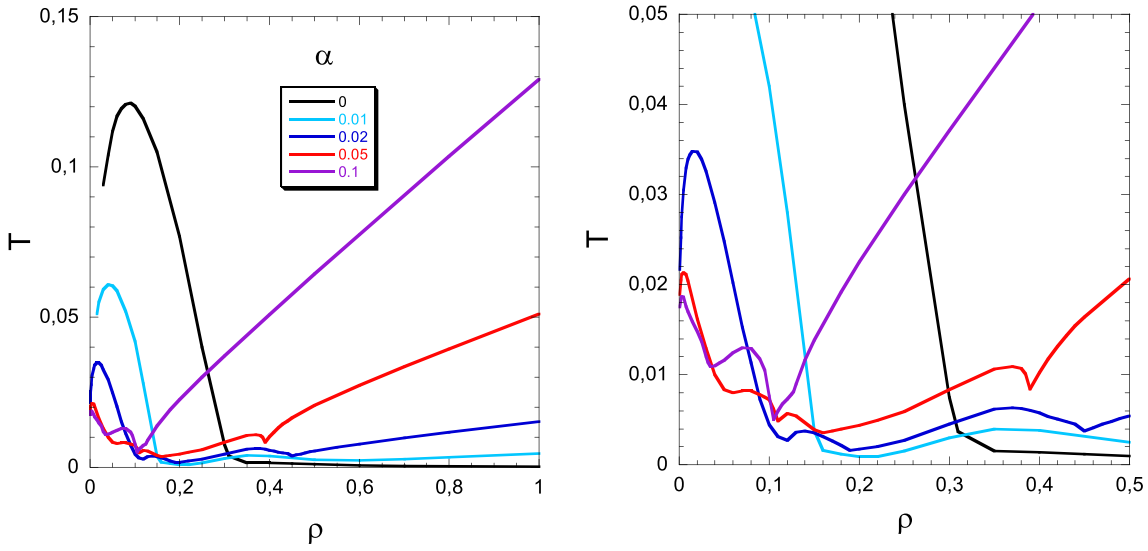

Fig. 12. Boundary line of the HNC equation in the temperature-density plane for several values of α. For each α, the region of instability of the theory is the portion of the plane laying below the corresponding line.

4.3. Phase behavior

As previously observed, there is a region of the thermodynamic plane where the HNC equation does not converge. In order to map the region of stability of the HNC equation, and thus, within the limits of this theoretical approach, of the stable fluid, we calculated the boundary line of the HNC equation (i.e. the line below which no solution to the equation can be found) for several values of the long-range repulsion strength α.

As shown in Fig. 12, the topology of the BL depends significantly on the strength α of the long range repulsion. When no long-range repulsion is present (i.e. for $\alpha = 0$) our model consists just in a Gaussian repulsive core supplemented by an attractive component. In this case, if attraction is strong enough, the system undergoes what has been called a thermodynamic catastrophe, i.e., particles will collapse to a finite volume of space since the bounded nature of the repulsive core is not able to withstand attractive interactions [37,38,55,56]. According to Ref. [55], a sufficient condition for thermodynamic instability is $\tilde{U}(0)<0$, with $\tilde{U}(k)$ being the Fourier transform of U(r); conversely, if $\tilde{U}(0)\geq 0$, for all k, then the system is stable. For the potential considered here, with $\alpha = 0$, we find $\tilde{U}(0)<0$ for $w > w_c \equiv 0.056\ldots$ (in ϵ units); below w_c, $\tilde{U}(k)$ is positive definite. Hence our system is stable for $w < w_c$. The specific case investigated ($w \cong 0.05$) corresponds then to a thermodynamically stable system. As shown in Fig. 12, the HNC boundary line for $\alpha = 0$ has a bell-shaped form similar to a typical liquid-gas spinodal line. When the long-range repulsion is turned on, the bell-shaped portion of the BL moves towards lower temperatures and becomes narrower, as expected due to the overall increase of repulsion and the consequent decreasing importance of the attractive component.

We report in Fig. 13 the structure factor at $\rho = 0.01$, for several values of α, at a temperature just above the boundary line. Since the BL changes with α, this temperature depends on α too. For $\alpha = 0$, S(k) has a local peak at $k = 0$, as it follows from the increase of the isothermal compressibility upon approaching the pseudo-spinodal. As α increases, the peak of S(k) at $k = 0$ gradually decreases, and a local peak develops at $k \neq 0$, i.e. the system goes from a simple fluid – like behavior to an "intermediate range order" behavior. Fig. 13 is qualitatively similar to Fig. 11 (panel referring to $\rho = 0.01$), but due to the proximity to the instability region, the peaks (and valleys) of S(k) are more pronounced. Moreover, it provides more accurate information about the nature of the instability region. For $\alpha = 0.02$, S(k) has a maximum at $k = 0$ (at difference from Fig. 11), whereas this is no more true for $\alpha = 0.03$. Thus we expect that the system turns from a liquid-gas transition behavior to a regime of instability with respect to mesoscale fluctuations for $0.02 < \alpha < 0.03$.

As discussed in Section 3.1, the region below the BL of the HNC equation has been associated for simple fluids with the liquid-gas spinodal, and thus to instability with respect to large scale density fluctuations. Accordingly, the peak of S(k) at $k = 0$ increases upon approaching the BL of simple fluids. As shown in Fig. 12, for the system investigated the BL is considerably more complex with respect to simple fluids. To get an insight into the meaning of the BL, we calculated the structure factor at a temperature just above the boundary line for a fixed α (0.05) and for several densities (see Fig. 14). Comparing Fig. 14 to the left panel of Fig. 2, we note that the peaks of S(k) attain considerably higher values. This holds for the two pre-peaks as well as for the first

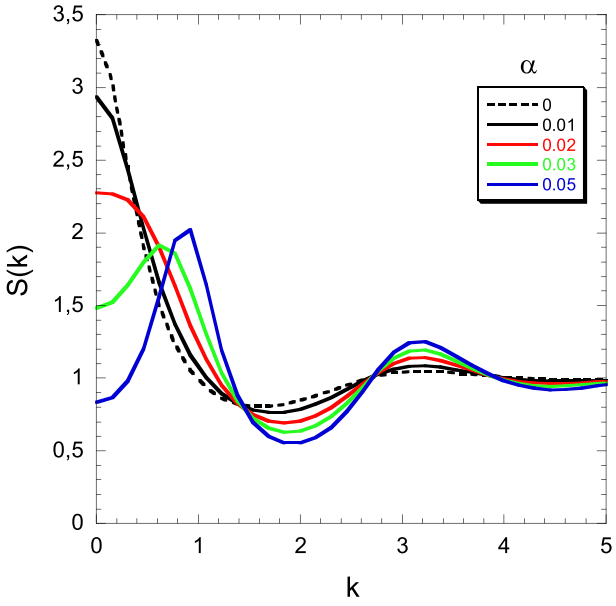

Fig. 13. Structure factor S(k) calculated through the HNC equation close to the boundary line, for several values of α, at $\rho = 0.01$. Temperatures at which S(k) is calculated: $\alpha = 0$, T = 0.061; $\alpha = 0.01$, T = 0.046; $\alpha = 0.02$, T = 0.034; $\alpha = 0.03$, T = 0.027; $\alpha = 0.05$, T = 0.021. The instability region was approached from high temperatures with temperature decrements as small as $\Delta T = 10^{-5}$.

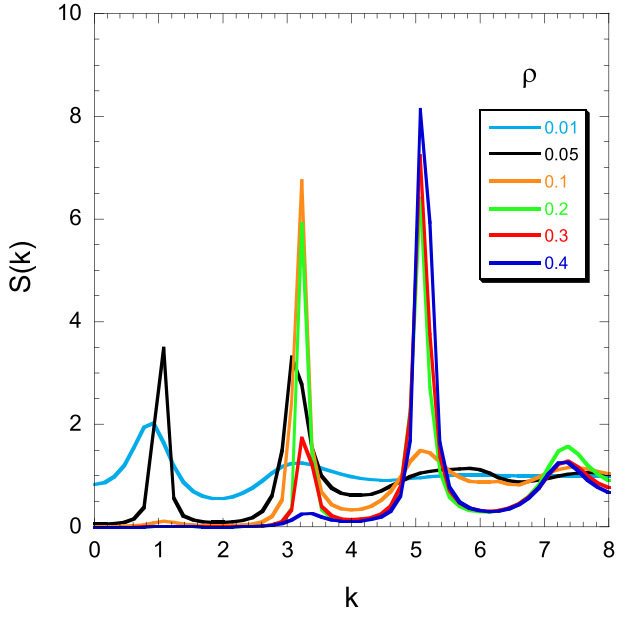

Fig. 14. Structure factor S(k) calculated through the HNC equation for $\alpha = 0.05$, close to the boundary line, at several densities. Temperatures at which S(k) is calculated: $\rho = 0.01$, T = 0.021; $\rho = 0.05$, T = 0.0083; $\rho = 0.1$, T = 0.0073; $\rho = 0.2$, T = 0.0044; $\rho = 0.3$, T = 0.0083; $\rho = 0.4$, T = 0.01; $\rho = 0.5$, T = 0.021. The instability region was approached from high temperatures with temperature decrements as small as $\Delta T = 10^{-5}$.

diffraction peak, depending on the value of the density. Thus, in the system investigated, the BL of the HNC equation is associated with the instability of the system with respect to density fluctuations whose characteristic scale decreases with the density. Such instability manifests itself in the increase of the peak corresponding to the scale that is more relevant at the density considered.

In order to investigate the system liquid-gas transition for $\alpha \neq 0$, we calculate the distribution of density fluctuations P(N,T,μ) using GCMC simulations (Fig. 15). In the one-phase region, P(N,T,μ) is a single-peak distribution in N, with a width related to the system compressibility and the average value indicating the equilibrium density at the selected T and μ values. In the two phase region P(N,T,μ) develops a double peak structure indicating the possibility of two different equilibrium states at the same value of μ. The value of μ for which the area below each peak is equal provides the value of μ at coexistence. As shown in the upper panel of Fig. 15, for $\alpha = 0.01$ a gas-liquid coexistence is clearly detected for T < 0.05. The estimated gas-liquid coexistence points are shown in Fig. 16 together with the HNC boundary line.

In order to locate the critical point, we compared the density fluctuations close to the critical point calculated through GCMC with the theoretical predictions of the fluctuations of the order parameter (properly scaled) in an Ising model at the critical point (Fig. 15, bottom panel). This allows us to identify $T = 0.0484 \pm 0.0001$ as the critical temperature, and $\rho = 0.056 \pm 0.003$ as the critical density. The corresponding critical value of the activity $e^{\beta\mu}$ is $8.11 \cdot 10^{-3}$.

As α increases, it is still possible to find some μ and T values for which P(N,T,μ) indicates two phases, even if the density of the less dense coexisting phase becomes extremely small. The shift of the phase diagram to very small densities imposes the use of larger and larger simulation boxes. In addition, a small-N peak arises, signaling the onset of finite size clusters. A finite size analysis in these cases is requested to separate cluster peaks (size independent) from density peaks (size dependent) [57]. For α larger than 0.023 we have not been able to clearly detect a gas-liquid coexistence. This is consistent with the behavior of S(k) shown in Fig. 13: for $\alpha = 0.02$ S(k) has a maximum at k = 0 whereas this is no more true for $\alpha = 0.03$.

When the long-range repulsion is turned on, in addition to the shrinking bell-shaped portion at low densities, the BL extends towards

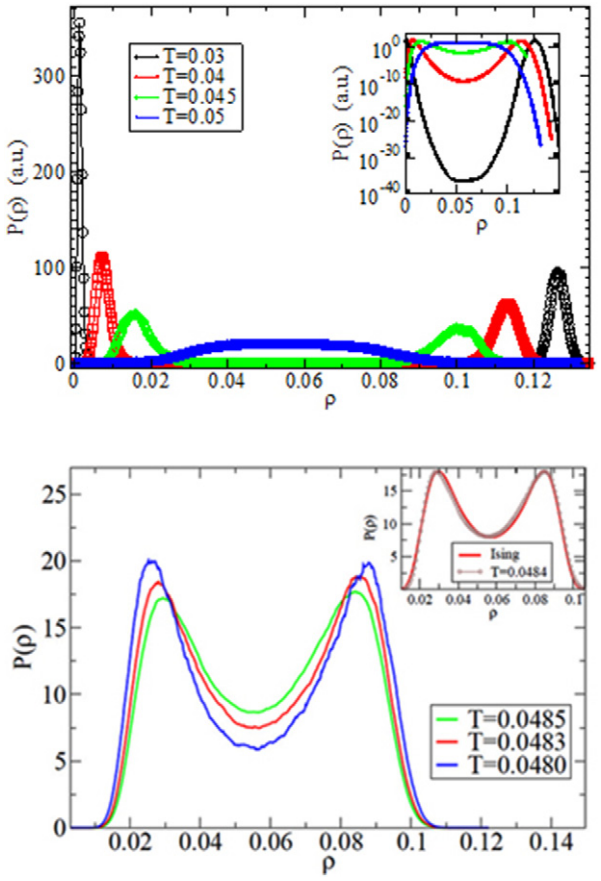

Fig. 15. Upper panel: distribution of the density fluctuations in a grand canonical Monte Carlo (GCMC) simulation; $\alpha = 0.01$. The side of the simulation box is L = 17. The inset shows the same data in log scale to highlight the free energy barrier separating the two phases. Bottom panel: density fluctuations calculated through GCMC simulation close to the critical point. The inset shows a comparison with the theoretical predictions of the fluctuations of the order parameter (properly scaled) in an Ising model at the critical point.

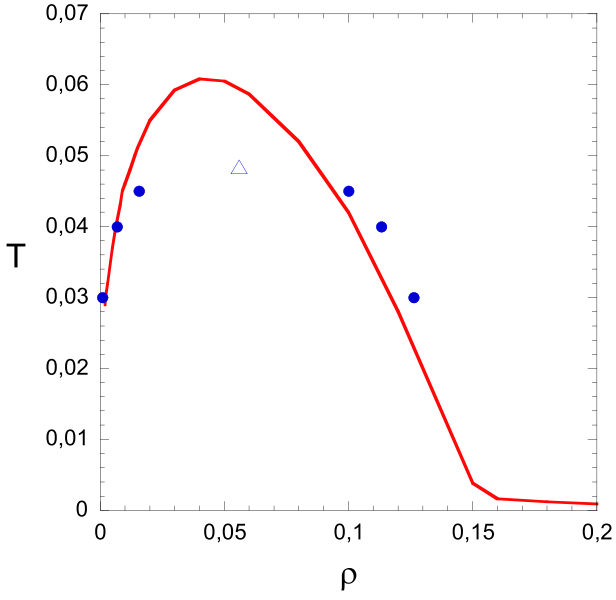

Fig. 16. Gas-liquid coexistence densities calculated through GCMC simulation (blue circles); the triangle represents the critical point estimated through the procedure described in the text. The HNC boundary line (solid red line) is reported for comparison. $\alpha = 0.01$.

intermediate and large densities (Fig. 12). In addition to the maximum at low densities, the BL develops also one or more local maxima at intermediate densities. At high densities, the BL tends to a straight line with a positive dT/dρ slope, which gets steeper and steeper with increasing α. This density dependence of the BL is similar to that of the BL of the penetrable sphere model (PSM) [40,41]. It has been shown that the crystallization of the PSM, and of other systems interacting through a bounded repulsion that decays fast enough to zero as the interparticle separation goes to infinity, is characterized by freezing into clustered crystals with multiple occupied sites [40,41]. On the contrary, in spite of the apparent similarity between the PSM and the GCM, the latter has a maximum freezing temperature, above which it remains fluid at all densities, while below this temperature it undergoes, with increasing density at constant temperature, a re-entrant melting into a high-density uniform fluid. The radically different phase behavior of the GCM and of the PSM is somewhat surprising, in the light of the apparent similarity between the two models. The reason for this difference is that in the PSM the particles can build clusters in which two or more particles occupy the same site, whereas in the GCM this event is not favored energetically.

Through a liquid state theory as the HNC equation it is not possible to investigate directly the nature of the solid state, but we can study the radial distribution function of the system in the fluid phase in order to find out incipient signals of the overlapping of particles. For example, from Fig. 2 we observe that g(r), in the point of the thermodynamic plane with coordinates ρ = 0.5, T = 0.03 (α = 0.05) shows a local maximum at r = 0, a signal of the partial overlapping of particles. This point lays in the fluid region not far from the high-density monotonically increasing portion of the BL corresponding to α = 0.05. Such local maximum at r = 0 is absent at lower densities (at T = 0.03).

In general, at a given temperature, overlapping of particles occurs only when density is sufficiently large. To investigate this point, we calculated the radial distribution function at a temperature just above the boundary line for α = 0.05 and for several densities, so to locate the density where the onset of overlapping occurs along the BL. We report in Fig. 17 the radial distribution function in the interval of densities of interest. At $\rho = 0.37$, g(r) is practically zero even at the smallest values of r. Overlapping of particles begins to be evident at $\rho = 0.38$, and a small density increment suffices in order that it becomes extremely relevant, as shown by the huge value of g(r = 0) at $\rho = 0.39$. Thus, the onset of overlapping close to the BL occurs rather abruptly. It can be

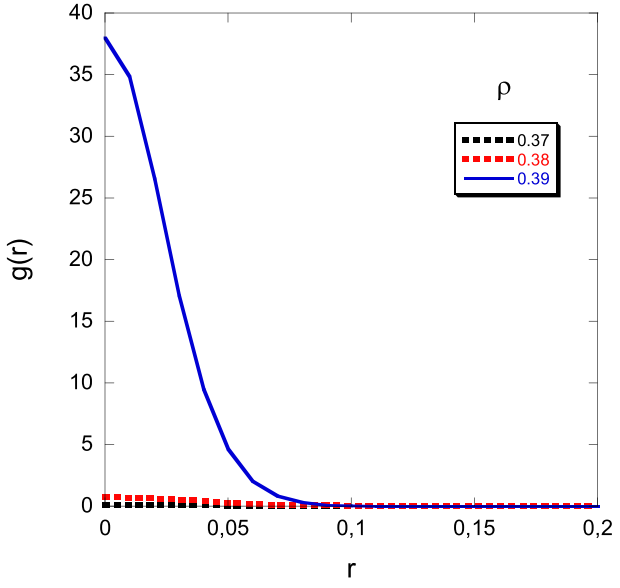

Fig. 17. Radial distribution function g(r) calculated through the HNC equation close to the boundary line, for $\alpha = 0.05$, for a few densities (the corresponding points in the thermodynamic plane are the circles in Fig. 18). The instability region was approached from high temperatures with temperature decrements as small as $\Delta T = 10^{-5}$.

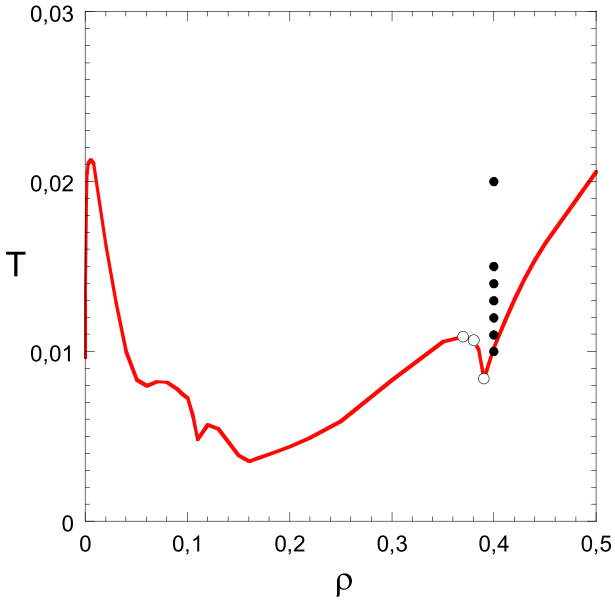

Fig. 18. Boundary line of the HNC equation for $\alpha = 0.05$. The circles correspond to the points with coordinates: $\rho = 0.37$, T = 0.01086; $\rho = 0.38$, T = 0.01068; $\rho = 0.39$, T = 0.00842. The dots correspond to the points with coordinates $\rho = 0.4$ and T = 0.02, 0.015, 0.014, 0.013, 0.012, 0.011, 0.01.

expected that, due to the disordering effect of temperature, at higher temperatures the onset of overlapping occurs more smoothly, and at higher densities.

To investigate the effect of temperature on the overlapping of particles, we calculated the radial distribution function for $\alpha = 0.05$, along the isochore $\rho = 0.4$. We know that for such density, close to the boundary line overlapping is quite relevant (Fig. 17). We start from a relatively high temperature and gradually decrease it so to approach the BL. As shown in Fig. 19, at T = 0.02 g(r) is zero inside the repulsive core (say, for $r < 1$) so there is no overlapping. By decreasing the temperature, overlapping becomes more and more relevant and eventually at T = 0.01, quite close to the BL, g(r) has a very high maximum for r = 0. It is to be noted that as the BL is approached more and more closely, the increase of g(r = 0) is more and more rapid (inset of Fig. 19).

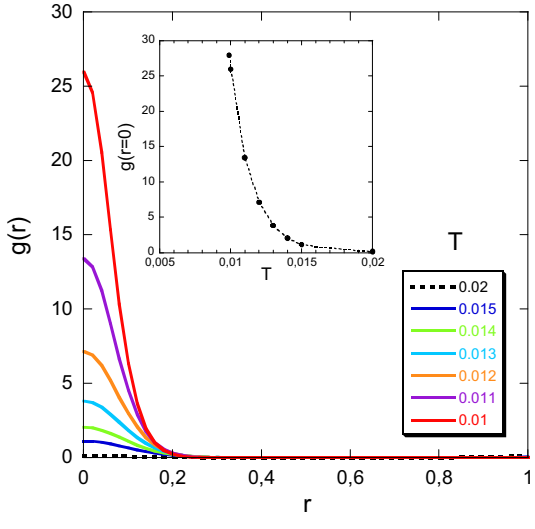

Fig. 19. Radial distribution function g(r) calculated through the HNC equation for $\alpha = 0.05$, at $\rho = 0.4$, and several temperatures (the corresponding points in the thermodynamic plane are the dots in Fig. 18). Inset: g(r = 0) as function of the temperature.

MD simulation makes it possible to calculate the radial distribution function also where the HNC no longer can be solved. As shown in Fig. 4 right panel, at $\rho = 0.5$ and $T = 0.01$ (i.e. inside the unstable region of the HNC equation) $g(r)$ has a very high maximum at $r = 0$, a clear sign of multiple occupancy of sites, and exhibits a solid-like alternation of peaks at larger distances. Both simulation and theoretical results support then the picture that the system considered undergoes at high densities freezing into a clustered solid. Thus, the presence of the interaction components added to the Gaussian repulsive core, i.e. the short range attraction and the long range repulsion, modify the freezing behavior that is typical of the Gaussian core when alone, and determines a tendency to form a clustered solid (this point is the object of an ongoing investigation).

5. Conclusions

We investigated the formation of aggregates in a system of particles interacting through a Gaussian repulsive core followed by an attractive well and a long-range repulsive component. Thus, at difference from other model fluids with competing short-range attraction and long-range repulsion (SALR systems) studied in the literature, the system considered has a bounded repulsive core rather than a diverging one. This feature makes it suited to model a number of systems that are relevant in soft matter, such as dendrimers, polymer chains, colloidal dispersions, and other flexible macromolecules.

Our calculations show that at low densities the system considered is formed by polydisperse clusters with a preferred cluster size. Concurrently, the structure factor exhibits a pre-peak at low wavevectors that can be associated with the emergence of intermediate range order (IRO). The low-k peak is a characteristic feature of many SALR systems and is generally considered as a necessary but not sufficient evidence for the presence of a clustered phase. Provided a cluster phase occurred, as in our case, the real-space length scale $2\pi/(k_{IRO})$, corresponding to the position k_{IRO} of the low-k pre-peak, can be interpreted as the average real-space intercluster distance.

At intermediate densities, the dominant feature in the structure factor of the system considered is a second pre-peak situated between the low-k peak and the main diffraction peak. This feature has never been reported for SALR model systems. According to the analysis here presented, this second pre-peak is associated to inter-particle correlations in which the LR repulsion plays a key role in generating partially excluded volume effects. A relevant consequence of such correlations is that in a density range, the occupancy of the second coordination shell with respect to the first one is significantly larger than for other densities. Given the finite nature of the LR repulsion, its efficacy to this regard tend to vanish at large densities.

Finally, at high densities, our system undergoes crystallization into a clustered solid with multiple occupied sites, a phenomenon that is known to occur in a class of systems interacting through a purely repulsive bounded potential, but was never studied in systems with competing interactions. As the freezing line is approached, the structure factor of the fluid phase is characterized by the more and more rapid increase of the main diffraction peak, related to monomer-monomer correlation, while the radial distribution function shows a more and more relevant peak at $r = 0$, a clear signal of particle overlapping.

Thus, as density varies, different length scales become effective in our system. This is reflected by the behavior of the structure factor, that is characterized by the turning on/off of the first and of the second pre-peaks, and by the rapid increase of the monomer-monomer peak at high densities.

CRediT authorship contribution statement

Gianpietro Malescio: Conceptualization, Methodology, Software, Validation, Formal analysis, Investigation, Resources, Data curation, Writing - original draft, Writing - review & editing, Visualization, Supervision, Project administration, Funding acquisition. **Francesco Sciortino:** Methodology, Software, Validation, Formal analysis, Investigation, Resources, Data curation, Writing - review & editing, Visualization, Supervision, Project administration, Funding acquisition.

Declaration of competing interest

The authors declare that they have no known competing financial interests or personal relationships that could have appeared to influence the work reported in this paper.

References

[1] M. Seul, D. Andelman, Domain shapes and patterns: the phenomenology of modulated phases, Science 267 (1995) 476–483.
[2] D. Langevin, Microemulsion, Acc. Chem. Res. 21 (1988) 255–260.
[3] E. Helfand, Block copolymers, polymer-polymer interfaces, and the theory of inhomogeneous polymers, Acc. Chem. Res. 8 (1975) 295–299.
[4] I.W. Hamley, Developments in Block Copolymer Science and Technology, Wiley, New York, 2004 1–29.
[5] F.S. Bates, G.H. Fredrickson, Block copolymers-designer soft materials, Phys. Today 52 (2) (1999) 32–38.
[6] H.C. Kim, S.M. Park, W.D. Hinsberg, Block copolymer based nanostructures: materials, processes, and applications to electronics, Chem. Rev. 110 (2010) 146–177.
[7] M.C. Goh, W.I. Goldburg, C.M. Knobler, Phase separation of a binary liquid mixture in a porous medium, Phys. Rev. Lett. 58 (1987) 1008–1011.
[8] R.B. Jadrich, K.S. Schweizer, Directing colloidal assembly and a metal-insulator transition using a quench-disordered porous rod template, Phys. Rev. Lett. 113 (2014), 208302.
[9] A. Yethiraj, A. van Blaaderen, A colloidal model system with an interaction tunable from hard sphere to soft and dipolar, Nature 421 (2003) 513–517.
[10] A. Stradner, H. Sedgwick, F. Cardinaux, W.C.K. Poon, S.U. Egelhaaf, P. Schurtenberger, Equilibrium cluster formation in concentrated protein solutions and colloids, Nature 432 (2004) 492–495.
[11] L. Porcar, P. Falus, W.R. Chen, A. Faraone, E. Fratini, K. Hong, P. Baglioni, Y. Liu, Formation of the dynamic clusters in concentrated lysozyme protein solutions, J. Phys. Chem. Lett. 1 (2010) 126–129.
[12] T. Lafitte, S.K. Kumar, A.Z. Panagiotopoulos, Self-assembly of polymer-grafted nanoparticles in thin films, Soft Matter 10 (2014) 786–794.
[13] D. Soraruf, F. Roosen-Runge, M. Grimaldo, F. Zanini, R. Schweins, T. Seydel, F. Zhang, R. Roth, M. Oettel, F. Schreiber, Protein cluster formation in aqueous solution in the presence of multivalent metal ions—a light scattering study, Soft Matter 10 (2014) 894–902.
[14] D. Pini, G. Jialin, A. Parola, L. Reatto, Enhanced density fluctuations in fluid systems with competing interactions, Chem. Phys. Lett. 327 (2000) 209–215.
[15] Y. Liu, W.R. Chen, S.H. Chen, Cluster formation in two-Yukawa fluids, J. Chem. Phys. 122 (2005), 044507.
[16] J.M. Bomont, J.L. Bretonnet, D. Costa, Temperature study of cluster formation in two-Yukawa fluids, J. Chem. Phys. 132 (2010), 184508.
[17] Y. Liu, L. Porcar, J. Chen, W.R. Chen, P. Falus, A. Faraone, E. Fratini, K. Hong, P. Baglioni, Lysozyme protein solution with an intermediate range order structure, J. Phys. Chem. B 115 (2011) 7238–7247.
[18] P.D. Godfrin, R. Castañeda-Priego, Y. Liu, N.J. Wagner, Intermediate range order and structure in colloidal dispersions with competing interactions, J. Chem. Phys. 139 (2013), 154904.
[19] P.D. Godfrin, N.E. Valadez-Perez, R. Castañeda-Priego, N.J. Wagner, Y. Liu, Generalized phase behavior of cluster formation in colloidal dispersions with competing interactions, Soft Matter 10 (2014) 5061–5071.
[20] Y. Liu, Colloidal systems with both a short-range attraction and a long-range repulsion, Chem. Eng. Process. Technol. 1 (2) (2013) 1010.
[21] P.D. Godfrin, S.D. Hudson, K. Hong, L. Porcar, P. Falus, N.J. Wagner, Y. Liu, Short-time glassy dynamics in viscous protein solutions with competing interactions, Phys. Rev. Lett. 115 (2015), 228302.
[22] F. Sciortino, S. Mossa, E. Zaccarelli, P. Tartaglia, Equilibrium cluster phases and low-density arrested disordered states: the role of short-range attraction and long-range repulsion, Phys. Rev. Lett. 93 (2004), 055701.
[23] J.C.F. Toledano, F. Sciortino, E. Zaccarelli, Colloidal systems with competing interactions: from an arrested repulsive cluster phase to a gel, Soft Matter 5 (2009) 2390–2398.
[24] A.I. Campbell, V.J. Anderson, J.S. van Duijneveldt, P. Bartlett, Dynamical arrest in attractive colloids: the effect of long-range repulsion, Phys. Rev. Lett. 94 (2005), 208301.
[25] C.L. Klix, C.P. Royall, H. Tanaka, Structural and dynamical features of multiple metastable glassy states in a colloidal system with competing interactions, Phys. Rev. Lett. 104 (2010), 165702.
[26] Y. Liu, Y. Xi, Colloidal systems with a short-range attraction and long-range repulsion: phase diagrams, structures, and dynamics, Curr. Opin. Colloid Interface Sci. 39 (2019) 123–136.
[27] Y. Zhuang, K. Zhang, P. Charbonneau, Equilibrium phase behavior of a continuous-space microphase former, Phys.Rev.Lett. 116 (2016) 98301.
[28] Y. Zhuang, P. Charbonneau, Equilibrium phase behavior of the square-well linear microphase-forming model, J. Phys. Chem. B 120 (2016) 6178–6188.

[29] E. Moaseri, J.A. Bollinger, B. Changalvaie, L. Johnson, J. Schroer, K.P. Johnston, T.M. Truskett, Reversible self-assembly of glutathione-coated gold nanoparticle clusters via pH-tunable interactions, Langmuir 33 (2017) 12244–12253.
[30] C.A.S. Cabezas, G.K. Ong, R.B. Jadrich, B.A. Lindquist, A. Agrawal, T.M. Truskett, D.J. Milliron, Gelation of plasmonic metal oxide nanocrystals by polymer-induced depletion attractions, PNAS 115 (2015) 8925–8930.
[31] D.J. Herr, Directed block copolymer self-assembly for nanoelectronics fabrication, J. Mater. Res. 26 (2011) 122–139.
[32] C.M. Bates, T. Seshimo, M.J. Maher, W.J. Durand, J.D. Cushen, L.M. Dean, G. Blachut, C.J. Ellison, C.G. Willson, Polarity-switching top coats enable orientation of sub-10-nm block copolymer domains, Science 338 (2012) 775–779.
[33] A.A. Louis, P.G. Bolhuis, J.P. Hansen, E.J. Meijer, Can polymer coils be modeled as "soft colloids", Phys. Rev. Lett. 85 (2000) 2522.
[34] C.N. Likos, M. Schmidt, H. Löwen, M. Ballauff, D. Pötschke, P. Lindner, Soft interaction between dissolved flexible dendrimers: theory and experiment, Macromolecules 34 (2001) 2914–2920.
[35] C.N. Likos, Effective interactions in soft condensed matter physics, Phys. Rep. 348 (2001) 267–439.
[36] J.P. Hansen, I.R. Mcdonald, Theory of Simple Liquids, Academic, London, 2006.
[37] G. Malescio, S. Prestipino, Phase behavior near and beyond the thermodynamic stability threshold, Phys.Rev.E 92 (2015) 050301(R).
[38] S. Prestipino, G. Malescio, Characterization of the structural collapse undergone by an unstable system of ultrasoft particles, Phys. A 457 (2016) 492–505.
[39] G. Malescio, A. Parola, S. Prestipino, Universal behavior of soft-core fluids near the threshold of thermodynamic stability, J. Chem. Phys. 148 (2018), 084904.
[40] C.N. Likos, M. Watzlawek, H. Löwen, Freezing and clustering transitions for penetrable spheres, Phys. Rev. E 58 (1998) 3135–3144.
[41] E. Lascaris, G. Malescio, S.V. Buldyrev, H.E. Stanley, Cluster formation, waterlike anomalies, and re-entrant melting for a family of bounded repulsive interaction potentials, Phys.Rev.E 81 (2010) 031201.
[42] G. Malescio, Phase stability of the penetrable-square-well model: an integral equation approach, Mol. Phys. 112 (2014) 1731–1735.
[43] P. Virnau, M. Müller, Calculation of free energy through successive umbrella sampling, J. Chem. Phys. 120 (2004) 10925–10930.
[44] T. Vissers, Z. Preisler, F. Smallenburg, M. Dijkstra, F. Sciortino, Predicting crystals of Janus colloids, J. Chem. Phys. 138 (2013), 164505.
[45] J. Russo, J.M. Tavares, P.I.C. Teixeira, M.T. da Gama, F. Sciortino, Reentrant phase diagram of network fluids, Phys. Rev. Lett. 106 (2011) 85703.
[46] A. Shukla, E. Mylonas, E. Di Cola, S. Finet, P. Timmins, T. Narayanan, D.I. Svergun, Absence of equilibrium cluster phase in concentrated lysozyme solutions, PNAS 105 (2008) 5075–5080.
[47] R.B. Jadrich, J.A. Bollinger, K.P. Johnston, T.M. Truskett, Origin and detection of microstructural clustering in fluids with spatial-range competitive interactions, Phys. Rev. E 91 (2015), 042312.
[48] J.A. Bollinger, T.M. Truskett, Fluids with competing interactions. I. Decoding the structure factor to detect and characterize self-limited clustering, J. Chem. Phys. 145 (2016), 064902.
[49] S. Li, J.L. Bañuelos, J. Guo, L. Anovitz, G. Rother, R.W. Shaw, P.C. Hillesheim, S. Dai, G.A. Baker, P.T. Cummings, Alkyl chain length and temperature effects on structural properties of pyrrolidinium-based ionic liquids: a combined atomistic simulation and small-angle X-ray scattering study, J. Phys. Chem. Lett. 3 (2012) 125–130.
[50] We note that Liu et al. [17] observed a (not very evident) second pre-peak, in addition to the first pre-peak, for a model system considerably more complex than SALR systems. The interaction considered consisted in a diverging repulsive core followed, with increasing r, by: a short-range attraction, a repulsive region, a shallow attractive well, and, finally, at very long distances, a slowly decaying repulsive tail.
[51] A. Triolo, O. Russina, B. Fazio, G.B. Appetecchi, M. Carewska, S. Passerini, Nanoscale organization in piperidinium-based room temperature ionic liquids, J. Chem. Phys. 130 (2009), 164521.
[52] A. Martinelli, M. Maréchal, Å. Östlund, J. Cambedouzou, Insights into the interplay between molecular structure and diffusional motion in 1-alkyl-3-methylimidazoliumionic liquids: a combined PFG NMR and X-ray scattering study, Phys. Chem. Chem. Phys. 15 (2013) 5510–5517.
[53] J.J. Hettige, H.K. Kashyap, H.V.R. Annapureddy, C.J. Margulis, Anions, the reporters of structure in ionic liquids, J. Phys. Chem. Lett. 4 (2013) 105–110.
[54] L. Aguilera, J. Volkner, A. Labrador, A. Matic, The effect of lithium salt doping on the nanostructure of ionic liquids, Phys. Chem. Chem. Phys. 17 (2015) 27082–27087.
[55] D. Ruelle, Statistical Mechanics: Rigorous Results, Imperial College Press, London, 1999.
[56] M.E. Fisher, D. Ruelle, The stability of many-particle systems, J. Math. Phys. 7 (1966) 260–270.
[57] A.D. Mackie, A.Z. Panagiotopoulos, I. Szleifer, Aggregation behavior of a lattice model for amphiphiles, Langmuir 13 (1997) 5022–5031.